







[¹⁸F]FDG Uptake and Expression of Immunohistochemical Markers Related to Glycolysis, Hypoxia, and Proliferation in Indeterminate Thyroid Nodules

Elizabeth J. de Koster¹  · Adriana C. H. van Engen-van Grunsven²  · Johan Bussink³  · Cathelijne Frielink¹ · Lioe-Fee de Geus-Oei^{1,4,5}  · Benno Kusters² · Hans Peters³  · Wim J. G. Oyen^{1,6,7}  · Dennis Vriens⁴  · On behalf of the EFFECTS trial study group

Received: 11 July 2022 / Revised: 21 September 2022 / Accepted: 23 September 2022 / Published online: 17 October 2022
© The Author(s) 2022

Abstract

Purpose The current study explored the association between 2-[¹⁸F]fluoro-2-deoxy-D-glucose ([¹⁸F]FDG) uptake and the quantitative expression of immunohistochemical markers related to glucose metabolism, hypoxia, and cell proliferation in benign and malignant thyroid nodules of indeterminate cytology.

Procedures Using a case–control design, 24 patients were selected from participants of a randomized controlled multicenter trial (NCT02208544) in which [¹⁸F]FDG-PET/CT and thyroid surgery were performed for Bethesda III and IV nodules. Three equally sized groups of [¹⁸F]FDG-positive malignant, [¹⁸F]FDG-positive benign, and [¹⁸F]FDG-negative benign nodules were included. Immunohistochemical staining was performed for glucose transporters (GLUT) 1, 3, and 4; hexokinases (HK) 1 and 2; hypoxia-inducible factor-1 alpha (HIF1 α); monocarboxylate transporter 4 (MCT4); carbonic anhydrase IX (CA-IX); vascular endothelial growth factor (VEGF); sodium-iodide symporter (NIS); and Ki-67. Marker expression was scored using an immunoreactive score. Unsupervised cluster analysis was performed. The immunoreactive score was correlated to the maximum and peak standardized uptake values (SUV_{max}, SUV_{peak}) and SUV_{max} ratio (SUV_{max} of nodule/background SUV_{max} of contralateral, normal thyroid) of the [¹⁸F]FDG-PET/CT using the Spearman's rank correlation coefficient and compared between the three groups using Kruskal–Wallis tests.

Results The expression of GLUT1, GLUT3, HK2, and MCT4 was strongly positively correlated with the SUV_{max}, SUV_{peak}, and SUV_{max} ratio. The expression of GLUT1 ($p=0.009$), HK2 ($p=0.02$), MCT4 ($p=0.01$), and VEGF ($p=0.007$) was statistically significantly different between [¹⁸F]FDG-positive benign nodules, [¹⁸F]FDG-positive thyroid carcinomas, and [¹⁸F]FDG-negative benign nodules. In both [¹⁸F]FDG-positive benign nodules and [¹⁸F]FDG-positive thyroid carcinomas, the expression of GLUT1, HK2, and MCT4 was increased as compared to [¹⁸F]FDG-negative benign nodules. VEGF expression was higher in [¹⁸F]FDG-positive thyroid carcinomas as compared to [¹⁸F]FDG-negative and [¹⁸F]FDG-positive benign nodules.

Conclusions Our results suggest that [¹⁸F]FDG-positive benign thyroid nodules undergo changes in protein expression similar to those in thyroid carcinomas. To expand the understanding of the metabolic changes in benign and malignant thyroid nodules, further research is required, including correlation with underlying genetic alterations.

Key words Thyroid Nodule · [¹⁸F]FDG-PET/CT · Immunohistochemistry · Glycolysis · Glucose Metabolism

Introduction

Positron emission tomography/computed tomography (PET/CT) using the glucose analogue 2-[¹⁸F]fluoro-2-deoxy-D-glucose ([¹⁸F]FDG) visualizes (increased)

metabolic activity in tissues and is successfully applied for the diagnosis, staging, and monitoring of many types of cancers and inflammatory disorders [1]. [¹⁸F]FDG-PET/CT exploits the Warburg effect, a well-known phenomenon in oncology describing the altered metabolism in malignancies: as compared to a low rate of glycolysis followed by oxidative phosphorylation in normal tissues, increased glycolysis and lactic fermentation is observed in cancer,

✉ Elizabeth J. de Koster
Lisanne.deKoster@radboudumc.nl

Extended author information available on the last page of the article

even in the abundance of oxygen and functioning mitochondria [2].

In differentiated thyroid carcinoma (DTC), higher [^{18}F]FDG uptake is associated with more aggressive histopathology, tumor dedifferentiation, BRAF^{V600E} mutations, and other features related to an adverse prognosis [3–7].

In thyroid nodules of indeterminate cytology (defined as Bethesda classification category III or IV), a *negative* [^{18}F]FDG-PET/CT accurately rules out malignancy with a 94% sensitivity and could avoid 40% of futile diagnostic surgeries for benign nodules [8, 9]. The specificity of [^{18}F]FDG-PET/CT in cytologically indeterminate thyroid nodules, however, is mere 40% as many benign nodules also show increased (false positive) [^{18}F]FDG uptake [9].

It is currently only partly understood which alterations in the glucose metabolism underly the differences in [^{18}F]FDG uptake among various types of benign and malignant thyroid nodules.

In tumorigenesis in general, increased glucose influx into the cell by increased expression of glucose transporters (GLUT) is considered the primary mechanism behind the upregulated glucose metabolism [10–12]. Next, upregulation of the enzyme hexokinase (HK) causes increased glucose phosphorylation as the initiating step in glycolysis. As [^{18}F]FDG-6-phosphate, in contrast to glucose-6-phosphate, cannot be degraded, HK activity results in increased accumulation of [^{18}F]FDG [10]. Although [^{18}F]FDG uptake cannot be considered a surrogate for tumor hypoxia, the expression of hypoxia-inducible factor-1 alpha (HIF1 α) has been associated with [^{18}F]FDG uptake [13–15]. HIF1 α is a major glycolytic transcription factor, regulating the expression of many hypoxia- and glycolysis-related enzymes, including GLUT, monocarboxylate transporter 4 (MCT4), and carbonic anhydrase IX (CA-IX) [16]. Whereas MCT4 transports the lactate formed during (an)aerobic glycolysis out of the cell, CA-IX neutralizes the accompanying pH disturbances by regulating the reversible hydration of carbon dioxide [13, 17–19]. MCT4 and CA-IX are also upregulated by intracellular acidification resulting from lactate formation following aerobic glycolysis [16, 20].

As a part of tumor growth and progression, [^{18}F]FDG uptake is also associated with increased cell proliferation, reflected by the expression of nuclear protein Ki-67, which, in turn, is associated with tumor aggressiveness [21–23]. Moreover, vascular endothelial growth factor (VEGF) promotes tumor cell growth and is one of the main factors involved in angiogenesis in cancer, induced by hypoxia through HIF1 α [24, 25]. As glucose delivery is a function of perfusion, VEGF expression and [^{18}F]FDG uptake are also associated in various cancer types [26, 27].

Finally, as [^{18}F]FDG uptake is related to tumor dedifferentiation in thyroid carcinoma, an inverse relationship is observed between [^{18}F]FDG and iodine uptake. While

the glucose metabolism enhances, dedifferentiating thyroid carcinomas gradually lose their functional iodine uptake, reflected by the loss of the basal membranous expression of the sodium-iodide symporter (NIS) [28–30].

The association between [^{18}F]FDG uptake and the expression of various metabolic markers has been investigated in papillary thyroid carcinoma (PTC) in a limited number of studies with mixed results [13, 21, 26, 31–34]. Studies in other benign and malignant thyroid nodules infrequently included [^{18}F]FDG-PET/CT data [17–19, 22, 26, 34–37]. To the best of our knowledge, no studies were previously performed in cytologically indeterminate thyroid nodules.

In the current study, we explored the association between [^{18}F]FDG uptake and the expression of immunohistochemical markers related to glucose transport, glucose metabolism, hypoxia, and cell proliferation in (hemi)thyroidectomy specimens of thyroid nodules with indeterminate cytology. We aimed to find correlations to explain why many benign thyroid nodules show increased [^{18}F]FDG uptake and why the specificity of [^{18}F]FDG-PET/CT is limited in indeterminate nodules, ultimately aiming to better understand the pathophysiology of these nodules.

Material and Methods

Study Design and Case Selection

The study included patients with a Bethesda III or IV thyroid nodule who underwent an [^{18}F]FDG-PET/CT scan of the neck and had diagnostic thyroid surgery in the context of their participation in the *Efficacy of FDG-PET in Evaluation of Cytological indeterminate Thyroid nodules prior to Surgery (EFFECTS)* trial. This prospective, randomized controlled multicenter trial included 132 patients and was performed in 15 hospitals in the Netherlands between July 2015 and December 2019 (Clinicaltrials.gov: NCT02208544). Inclusion criteria and comprehensive study procedures of this trial were previously described [9]. For the current explorative study, including post hoc analyses of the trial data, an individually matched case–control design was chosen. We aimed to include 24 patients in three groups: eight true positives (TP), defined as patients with a visually [^{18}F]FDG-positive and histopathologically malignant index nodule (i.e., differentiated (non-medullary) thyroid carcinoma), eight false positives (FP), defined as patients with a visually [^{18}F]FDG-positive and histopathologically benign index nodule, and eight true negatives (TN), defined as patients with a visually [^{18}F]FDG-negative and histopathologically benign index nodule. [^{18}F]FDG-negative, histopathologically malignant index nodules (i.e., false negative [^{18}F]FDG-PET/CT) are rare and were not selected for the current study [9]. Prior to any immunohistochemical study procedures,

patients were selected for the current study from the original trial cohort by two of the researchers (EK and DV) based on the best possible match of individual patients between the three study groups while securing a balanced selection of histopathological diagnoses within groups, representative for the diagnoses found in the original trial and with a representative range in the degree of [^{18}F]FDG uptake (expressed as the maximum standardized uptake value, or SUV_{max} , in g/mL) per diagnosis [9]. Between groups, patients were matched based on sex, age at the time of the [^{18}F]FDG-PET/CT scan, histopathological size of the index nodule, and the presence of Hürthle cells in the histopathology sample. TP and FP cases were additionally matched based on the SUV_{max} of the index nodule. Patients were not eligible for inclusion in the current study if the thyroid nodule was smaller than 10 mm (due to possible limitations regarding the spatial resolution of the PET/CT scanner), if there was either an [^{18}F]FDG-positive hotspot within an [^{18}F]FDG-positive nodule or central photopenia (to limit the possibility of sampling error), if the [^{18}F]FDG-PET/CT images showed signs of thyroiditis throughout the thyroid including the index nodule, if the last fine needle aspiration cytology procedure (FNAC) and [^{18}F]FDG-PET/CT scan were less than 4 weeks apart (i.e., to limit the possibility of [^{18}F]FDG-positivity due to reactive tissue damage repair changes following FNAC), if no histopathology was available (i.e., following patient treatment allocation in the *EffECTS* trial), and/or if review of the histopathology showed signs of lymphocytic thyroiditis or necrosis in the index nodule (i.e., to limit the possibility of false positive or false negative [^{18}F]FDG-PET/CT readings, respectively).

The trial, including the current secondary analysis, was approved by the Medical Research Ethics Committee on Research Involving Human Subjects region Arnhem-Nijmegen, Nijmegen, the Netherlands. Written informed consent was obtained from each of the participants prior to any study activities.

FDG-PET/CT Acquisition, Reconstruction, and Analysis

During the *EffECTS* trial, all participants underwent a single [^{18}F]FDG-PET/CT of the neck. Scans were acquired by 20 different scanners at 12 EARL-accredited study sites using a standard acquisition and reconstruction protocol in accordance with European Association of Nuclear Medicine (EANM) guidelines [1]. Patients fasted for at least 6 h, and serum glucose levels were between 4 and 11 mmol/L. PET acquisition was scheduled 60 (55–75) min after intravenous bolus administration of [^{18}F]FDG. The administered activity was dependent on body weight, scan speed, bed overlap, and scanner sensitivity, equivalent to 3.45 MBq/kg (4 min/bed, < 25% bed overlap). Low-dose, non-contrast-enhanced

CT (IdCT) scans were acquired for attenuation correction of PET images.

All scans were centrally assessed by two independent, experienced nuclear medicine physicians (DV, LF). They were blinded to patient allocation and all clinical and cytological data except for the ultrasonographic size and location of the index nodule, to ensure its correct identification. For the visual assessment, any focal [^{18}F]FDG uptake within the thyroid that was visually higher than the physiological background [^{18}F]FDG uptake of the surrounding normal thyroid tissue and that corresponded to the index nodule in size and location was considered positive (Fig. 1). Quantitative image analyses were performed using OsiriX Lite DICOM-viewer (Pixmeo SARL, Bernex, Switzerland). SUV computation was validated after each mandatory software version update. The SUV_{max} and peak SUV (SUV_{peak} , defined as the maximum average SUV within a 1 cm³ spherical volume) of the index nodule were semi-automatically measured. Body weight-corrected values were used. The SUV_{max} ratio was calculated by dividing the SUV_{max} of the nodule by the background SUV_{max} of normal thyroid tissue in the contralateral lobe. [^{18}F]FDG-positive foci in the thyroid that did not correspond to the index nodule in size and location (i.e., thyroid incidentalomas) were not analyzed in the current study.

Histopathology

During the *EffECTS* trial, all postoperative patient management was based on the *local* histopathological diagnosis. For scientific purposes and to limit the effect of any inter-observer variability, all (hemi)thyroidectomy specimens were *centrally* reviewed by a dedicated thyroid pathologist (AE) in accordance with the WHO classification (4th edition) [38]. In case of discordance with the local diagnosis, an additional dedicated thyroid pathologist (BK) was consulted to reach consensus. Local and central histopathologists were blinded to the [^{18}F]FDG-PET/CT result; the two central pathologists were also blinded to the local histopathological diagnosis. Incidentally detected (micro)carcinomas located outside the index nodule were not considered for the main outcome measure.

Immunohistochemistry

Indirect chromogenic immunohistochemical staining was performed on 5- μm thick paraffin-embedded tissue sections on coated slide glasses. We used primary antibodies against GLUT1 (RB-9052-P, Thermo Fisher Scientific, Waltham, MA, USA; dilution 1:500), GLUT3 (RB-9096-P, Immunologic, WellMed BV, Duiven, the Netherlands; 1:300), GLUT4 (ab654, Abcam, Cambridge, UK: 1:1000), HK1 (MA5-15,680, Invitrogen™, Thermo Fisher Scientific; 1:7500), HK2 (MA5-15,679, Invitrogen™, Thermo Fisher

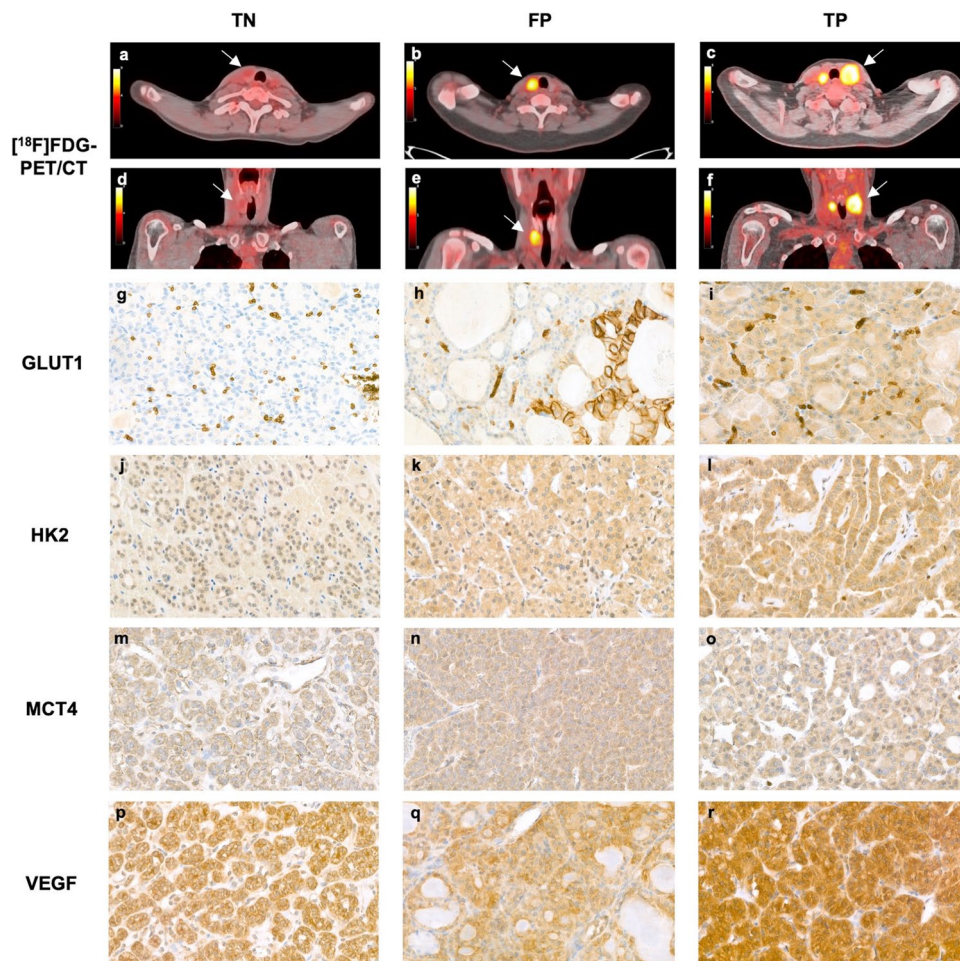


Fig. 1 Representative [^{18}F]FDG-PET/CT images and immunohistochemical staining patterns for the three groups. Transverse and coronal [^{18}F]FDG-PET/CT images of a right-sided, 19-mm, visually [^{18}F]FDG-negative follicular adenoma (TN group) with a SUV_{max} of 2.2 g/mL (**a**, **d**), a right-sided, 25-mm, visually [^{18}F]FDG-positive follicular adenoma (FP group) with a SUV_{max} of 8.0 g/mL (**b**, **e**), and a left-sided, 40-mm, visually [^{18}F]FDG-positive minimally invasive FTC (pT2N0Mx, TP group) with a SUV_{max} of 10.0 g/mL (with contralateral [^{18}F]FDG-positive multinodular goiter) (**c**, **f**). Illustrative, representative microscopy images ($\times 40$) of the immunohistochemistry stains observed in each of the groups show absent GLUT1 (**g**), weak HK2 (**j**), weak MCT4 (**m**), and intermediate VEGF (**p**) expression in TN nodules; weak cytoplasmic GLUT1 (**h**), intermediate HK2

(**k**), intermediate MCT4 (**n**), and intermediate VEGF (**q**) expression in FP nodules; and intermediate GLUT1 (**i**), intermediate HK2 (**l**), intermediate MCT4 (**o**), and strong VEGF (**r**) expression in TP nodules. In addition, several FP and TP nodules showed strong membranous GLUT1 expression in $< 10\%$ of cells (**h**). Note: the [^{18}F]FDG-PET/CT images and microscopy images in each column represent multiple patients from each group to represent the average findings per group; single patients with immunohistochemistry results consistent with the group average were not available. FP, false positives. FTC, follicular thyroid carcinoma. GLUT, glucose transporter. HK, hexokinase. MCT4, Monocarboxylate transporter 4. SUV_{max} , maximum standardized uptake value. TN, true negatives. TP, true positives. VEGF, vascular endothelial growth factor.

Scientific; 1:200), HIF1 α (ab2185, Abcam; 1:250), MCT4 (anti SLC16A4, HPA046986, Sigma-Aldrich®, Saint Louis, MO, USA; 1:200), CA-IX (NB100-417, Novus Biologicals™, Bio-technie, Centennial, CO, USA; 1:250), VEGF (555,036, Pharmingen™, Becton Dickinson Biosciences, San Diego, CA, USA; 1:100), NIS (ABC1453, Merck Millipore, Burlington, MA, USA; 1:2000), and Ki-67 (M724001, DAKO Agilent, Santa Clara CA, USA; 1:25).

Tissue sections were deparaffinized and rehydrated. Next, GLUT1, GLUT3, HIF1 α , CA-IX, and Ki-67 staining was performed using a semi-automated immunostainer

(Thermo Scientific, Labvision™ 488) following a standardized protocol according to manufacturer instructions. GLUT4, HK1, HK2, MCT4, VEGF, and NIS staining was performed manually. Detailed immunohistochemistry procedures are provided in the Supplementary data. In summary, antigen retrieval was performed, non-specific immunoreactivity was blocked, and slides were subsequently incubated with primary and secondary antibodies. Slides were incubated using 3,3-diaminobenzidine (DAB) as chromogen. Negative control samples were processed without primary antibodies. Positive control tissues were

Table 1 Baseline characteristics^a

	TN <i>n</i> = 8	FP <i>n</i> = 8	TP <i>n</i> = 8	<i>p</i>
Female	6 (75%)	5 (63%)	5 (63%)	0.83 ^b
Age (years) (mean ± SD)	51.2 ± 12.3	54.0 ± 11.8	54.2 ± 20.3	0.91 ^c
Nodule size on histopathology, mm (median, IQR)	33 (25–45)	26 (21–43)	35 (21–44)	0.83 ^d
Thyroid function				
TSH, mU/L (median, IQR)	1.20 (0.46–2.05)	1.65 (0.98–2.80)	1.55 (1.18–1.75)	0.21 ^d
fT4, pmol/L (median, IQR)	16.1 (13.6–17.4)	14.1 (13.3–15.5)	13.8 (12.0–19.8)	0.53 ^d
¹⁸ F]FDG-PET/CT scan				
SUV _{max} (g/mL) (median, IQR)	2.1 (1.2–2.3)	7.0 (4.5–31.0)	11.1 (4.2–20.8)	< 0.001 ^{d,e}
SUV _{peak} (g/mL) (median, IQR)	1.7 (1.0–2.1)	4.8 (4.0–24.6)	9.6 (2.8–15.8)	0.002 ^{d,e}
SUV _{max} -ratio (median, IQR)	1.0 (0.8–1.2)	4.3 (2.3–14.3)	6.2 (1.6–14.0)	< 0.001 ^{d,e}
Histopathological diagnosis				
Hyperplastic nodule	4 (50%)	2 (25%)		
Follicular adenoma	4 (50%)	4 (50%)		
Hürthle cell adenoma		2 (25%)		
PTC			2 (25%)	
FVPTC			1 (12.5%)	
FTC, minimally invasive			3 (37.5%)	
HCC, minimally invasive			2 (25%)	
TNM stage				
T1a			0 (0%)	
T1b			2 (25%)	
T2			4 (50%)	
T3			2 (25%)	
N0/x			6 (75%)	
N1a			2 (25%)	

FP, false positives. FTC, follicular thyroid carcinoma. FVPTC, follicular variant PTC. HCC, Hürthle cell carcinoma. IQR, interquartile range. PTC, papillary thyroid carcinoma. SD, standard deviation. TN, true negatives. TP, true positives

^aIndividual patient characteristics are presented in Supplementary Table 2

^bPearson's chi-squared

^cOne-way ANOVA

^dKruskal-Wallis test

^ePost hoc analysis: SUV_{max} $p = 0.001^*$ between TN and FP groups, $p < 0.001^*$ between TN and TP groups, and $p = 0.89$ between FP and TP groups; SUV_{peak} $p = 0.003^*$ between TN and FP groups, $p = 0.001^*$ between TN and TP groups, and $p = 0.83$ between FP and TP groups; SUV_{max}-ratio $p = 0.001^*$ between TN and FP groups, $p < 0.001^*$ between TN and TP groups, and $p = 0.89$ between FP and TP groups

used as recommended by the manufacturer. Finally, slides were counterstained with hematoxylin and dehydrated.

All slides were reviewed to quantify the expression of the immunohistochemical markers by evaluating the DAB staining by two members of the research team (EK and AE), who were blinded to the clinical data and [¹⁸F]FDG-PET/CT results (Fig. 1). The staining was assessed using the Remmele and Stegner immunoreactive score (IRS) by multiplying the staining intensity (score 0–3: negative, weak, intermediate, strong) with the proportion of stain-positive cells in the index nodule (score 0–4: 0%, 1–10%, 11–50%, 51–80%, > 80%) (Supplementary Table 1) [39]. Consequently, the minimum

IRS of 0 represents absent staining, and the maximum IRS of 12 represents strong staining in a majority of cells in the lesion. For the Ki-67 stain, the proliferation index was assessed as the percentage of cells with positive nuclear staining (score 1–3: < 3%, 3–5%, > 5%) among at least four representative fields of 100 tumor cells.

Statistical Analysis

Baseline characteristics were compared between the allocated groups using Pearson's chi-square for categorical

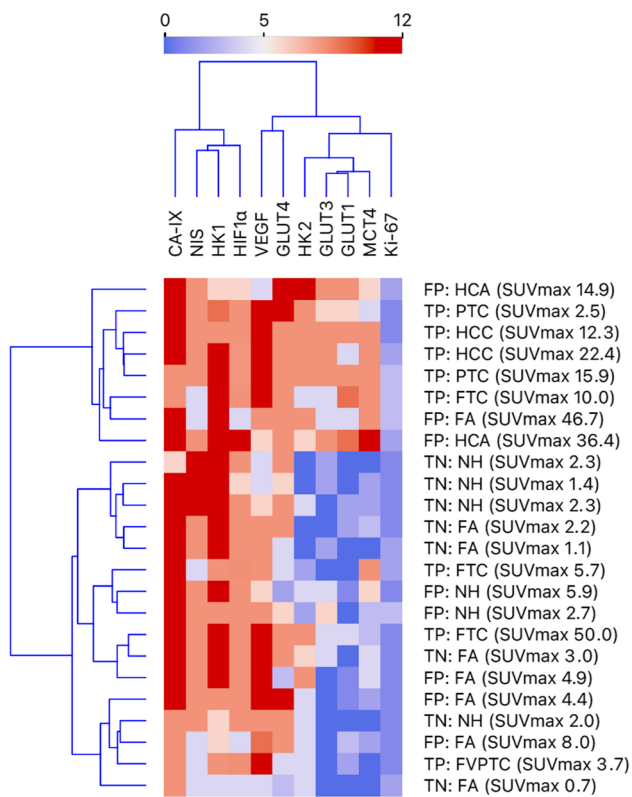


Fig. 2 Dendrogram heatmap showing the unsupervised cluster analysis of all 11 immunohistochemical stains of the 24 thyroid nodules, including the group, histopathological diagnosis, and SUV_{max} of these nodules. The IRS is presented on a scale from 0 (dark blue, absent stain) to 12 (dark red, strong stain in <80% of tumor cells). CA-IX, carbonic anhydrase IX. FA, follicular adenoma. FP, false positives. FTC, follicular thyroid carcinoma. FVPTC, follicular variant PTC. GLUT, glucose transporter. HCA, Hürthle cell adenoma. HCC, Hürthle cell carcinoma. HIF1 α , Hypoxia-inducible factor-1 alpha. HK, hexokinase. IRS, immunoreactive score. MCT4, Monocarboxylate transporter 4. NH, nodular hyperplasia. NIS, sodium-iodide symporter. PTC, papillary thyroid carcinoma. SUV_{max} , maximum standardized uptake value. TN, true negatives. TP, true positives. VEGF, vascular endothelial growth factor.

data and one-way ANOVA or Kruskal–Wallis tests for continuous data, where appropriate. Unsupervised cluster analysis with ordered leaves was performed using the IRS of all stains and Ki-67 proliferation index and visualized in a dendrogram with heat map. The IRS of all stains was correlated with each other, the SUV_{max} , SUV_{peak} , and SUV_{max} ratio using the Spearman's rank correlation coefficient with its degrees of freedom ($r_s[df]$). Next, the IRS of all immunomarkers was compared between TN, FP, and TP groups using Kruskal–Wallis (omnibus) tests and visualized using violin plots. In case the Kruskal–Wallis test indicated statistical significance, Dunn's post hoc tests were used for each pair of groups, and p values are presented. Counteracting for multiple comparisons was performed using Bonferroni correction; statistical

significance after correction is indicated by an asterisk (*). A p value of 0.05 or less was considered statistically significant. Statistical analysis was performed using IBM SPSS Statistics version 27 (IBM Corp., Armonk, NY, USA) and Orange: Data Mining Toolbox version 3.30.2 (Bioinformatics Lab, University of Ljubljana, Slovenia) [40].

Results

Twenty-four patients were included, of which 16 (67%) were female. The mean age was 53.1 ± 14.7 years. The median nodule size was 30 mm (interquartile range 24–45). SUV_{max} , SUV_{peak} , and SUV_{max} ratio were statistically significantly different between the groups (Table 1). These differences were significant between TN and FP and between TN and TP groups, but not between FP and TP groups.

Unsupervised cluster analysis (Fig. 2) indicated fair clustering of nodules in TN, FP, and TP groups based on the IRS of the 11 immunomarkers. Many lesions with a high SUV_{max} appeared to have a high expression of multiple markers, including FP as well as TP nodules.

The expression of multiple markers moderately positively correlated with each other: GLUT1 to GLUT3, GLUT4, HK2, and MCT4; GLUT3 to HK2, MCT4, and Ki-67; HK1 to NIS; HK2 to GLUT4, MCT4, and VEGF; and MCT4 to Ki-67 (Fig. 3).

The expression of GLUT1, GLUT3, HK2, and MCT4 was strongly positively correlated with the SUV_{max} , SUV_{peak} , and SUV_{max} ratio (Table 2). For GLUT1, both its cytoplasmic ($r_s(22) = 0.715$, $p < 0.001$) and membranous ($r_s(22) = 0.450$, $p = 0.03$) expressions were related to the SUV_{max} . For GLUT3, only its cytoplasmic expression was correlated with the SUV_{max} ($r_s(22) = 0.649$, $p < 0.001$).

The expression of GLUT1, HK2, MCT4, and VEGF was statistically significantly different between the TN, FP, and TP groups (Fig. 4). Post hoc analysis demonstrated that the expression of GLUT1, HK2, and MCT4 was similarly increased in FP and TP nodules as compared to the expression in TN nodules. VEGF expression was higher in TP as compared to both TN and FP nodules. VEGF expression was similar in TN and FP groups.

Discussion

When performing and interpreting [^{18}F]FDG-PET/CT scans, we should aim to understand the underlying pathophysiological processes at a cellular and molecular level. In indeterminate thyroid nodules, the specificity of



Fig. 3 Spearman’s rank correlation coefficients (r_s , $df=22$) of the IRS of the 11 immunohistochemical markers, presented on a color scale from -1 (dark blue) to 1 (dark red). CA-IX, carbonic anhydrase IX. GLUT, glucose transporter. HIF1 α , Hypoxia-inducible factor-1 alpha.

HK, hexokinase. IRS, immunoreactive score. MCT4, Monocarboxylate transporter 4. NIS, sodium-iodide symporter. VEGF, vascular endothelial growth factor.

[^{18}F]FDG-PET/CT is limited, as many benign nodules also show increased [^{18}F]FDG uptake [9]. The current explorative study demonstrated that [^{18}F]FDG uptake in indeterminate thyroid nodules was positively correlated with the expression of GLUT1, GLUT3, HK2, and MCT4. [^{18}F]FDG-positive benign thyroid nodules and

[^{18}F]FDG-positive thyroid carcinomas with indeterminate cytology showed increased expression of GLUT1, HK2, and MCT4 as compared to the expression in [^{18}F]FDG-negative benign nodules. The expression of VEGF was similar in [^{18}F]FDG-positive and [^{18}F]FDG-negative benign nodules, which was lower than in [^{18}F]

Table 2 Correlations between the IRS and SUV

IHC stain	SUV _{max}		SUV _{peak}		SUV _{max} ratio	
	r_s	p	r_s	p	r_s	p
GLUT1	0.731	<0.001	0.731	<0.001	0.720	<0.001
GLUT3	0.579	0.003	0.556	0.005	0.582	0.003
GLUT4	0.301	0.15	0.315	0.13	0.294	0.16
HK1	0.182	0.40	0.237	0.27	0.096	0.66
HK2	0.695	<0.001	0.681	<0.001	0.707	<0.001
HIF1 α	0.102	0.64	0.111	0.61	0.124	0.56
MCT4	0.760	<0.001	0.765	<0.001	0.740	<0.001
CA-IX	0.152	0.48	0.113	0.60	0.166	0.44
VEGF	0.373	0.07	0.393	0.054	0.359	0.09
NIS	-0.270	0.20	-0.270	0.20	-0.262	0.22
Ki-67	0.319	0.13	0.275	0.19	0.354	0.09

CA-IX, carbonic anhydrase IX. GLUT, glucose transporter. HIF1 α , Hypoxia-inducible factor-1 alpha. HK, hexokinase. IRS, immunoreactive score. MCT4, Monocarboxylate transporter 4. NIS, sodium-iodide symporter. r_s , Spearman’s rank correlation coefficient ($df=22$). SUV, standardized uptake value. VEGF, vascular endothelial growth factor

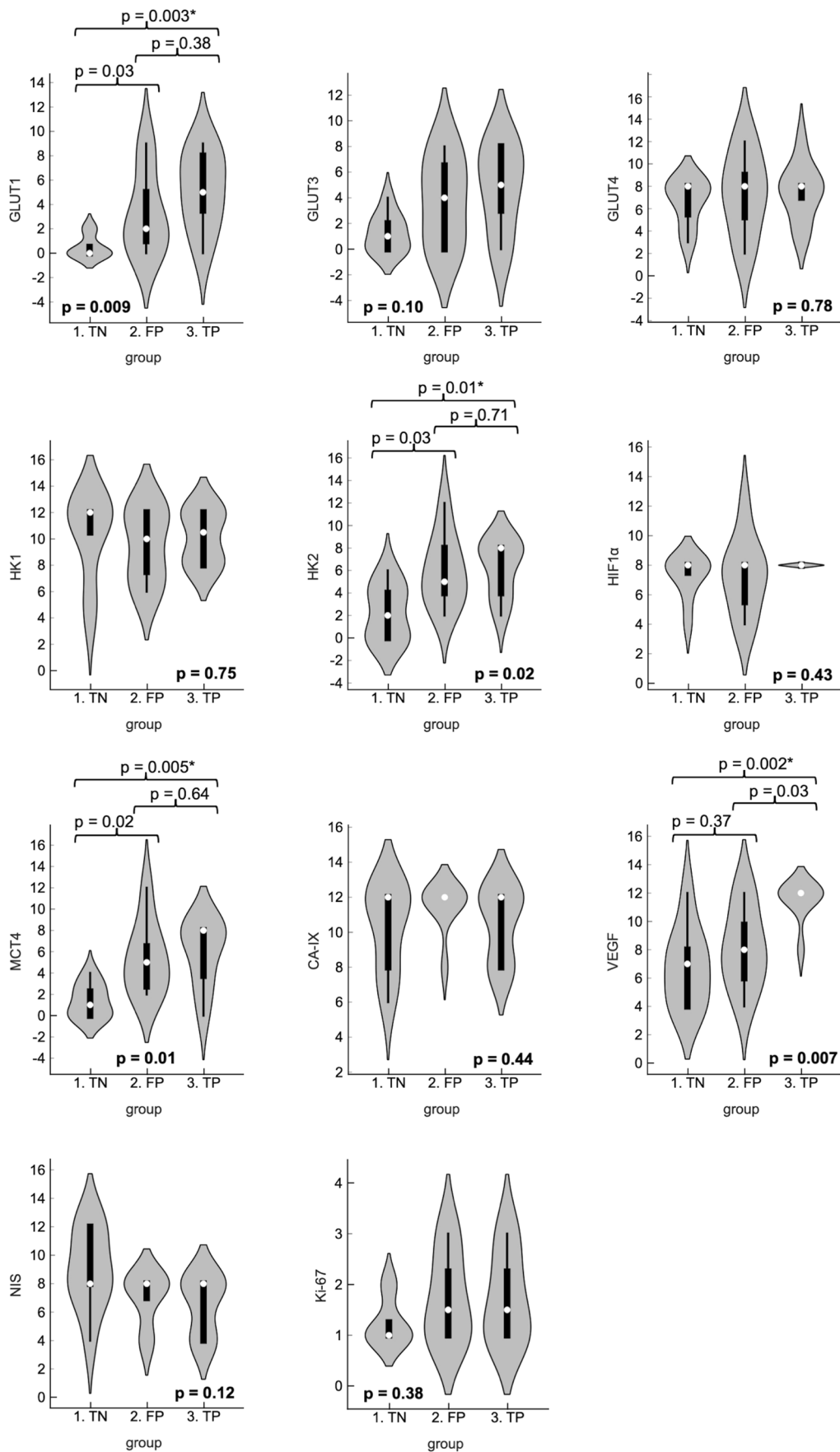


Fig. 4 Violin plots demonstrating the between-group comparison of the IRS of all IHC stains, including the median (white dot), inter-quartile range (thick black whisker), range (thin black whisker), and density based on counts (kernel). The boldfaced *p* value (bottom of each plot) represents the overall *p* value (Kruskal–Wallis test). The horizontal braces and corresponding *p* values represent the *p* values between two groups (post hoc Dunn’s test). Single asterisk (*) indicates statistical significance after Bonferroni correction for multiple comparisons. CA-IX, carbonic anhydrase IX. FP, false positives. GLUT, glucose transporter. HIF1 α , Hypoxia-inducible factor-1 alpha. HK, hexokinase. IRS, immunoreactive score. MCT4, Monocarboxylate transporter 4. NIS, sodium-iodide symporter. TN, true negatives. TP, true positives. VEGF, vascular endothelial growth factor.

FDG-positive thyroid carcinomas. GLUT3 expression was strongly correlated with the SUV metrics, but not statistically significantly different between the TN, FP, and TP groups in the current dataset. These results indicate that glucose metabolism-related alterations in the protein expression of [^{18}F]FDG-positive benign thyroid nodules may be similar to alterations occurring in thyroid carcinomas, at least in those deriving from cytologically indeterminate nodules.

To the best of knowledge, our study is the first to assess immunohistochemical staining for metabolic markers in comparison to [^{18}F]FDG-PET/CT results in cytologically indeterminate thyroid nodules.

The previous, heterogeneous studies of these markers in thyroid carcinomas showed mixed results, possibly hindered by their oftentimes limited sample size and statistical power [21, 26, 33, 34]. An increased expression of GLUTs and HKs was observed in PTC and to a lesser extent in follicular thyroid carcinoma (FTC) as compared to follicular adenoma (FA) and normal thyroid tissue [18, 35, 36, 41]. An association between [^{18}F]FDG uptake and the increased expression of GLUTs and HKs was previously observed in DTC but remained unconfirmed in the latest studies [13, 21, 26, 31–34]. [^{18}F]FDG-positive PTC showed a higher expression of HIF1 α as compared to [^{18}F]FDG-negative PTC [13]. Higher expression of MCT4 and CA-IX was previously found in poorly differentiated and anaplastic thyroid carcinoma as compared to PTC and FTC and in FTC as compared to FA [18, 19]. MCT4 was not previously associated to [^{18}F]FDG uptake in thyroid neoplasms. Increased expression of VEGF was observed in both PTC and FTC as compared to FA and multinodular goiter [24, 33, 42]. In PTC and FTC, CA-IX, VEGF, and NIS expression appeared unrelated to [^{18}F]FDG uptake [26, 33, 34]. The Ki-67 proliferation index was higher in FTC than FA [37]. In a single study, the Ki-67 proliferation index was also associated with the SUV_{max} in PTC [21].

The current study does not resolve the origin of the enhanced glucose metabolism and increased [^{18}F]FDG uptake in the malignant and part of the benign thyroid

nodules. In thyroid carcinomas, [^{18}F]FDG uptake likely reflects metabolic alterations caused by oncogenic mutations in various pathways. In PTC, the presence of a BRAF^{V600E} mutation is associated with [^{18}F]FDG uptake and with over-expression of GLUT1, GLUT3, HK2, HIF1 α , MCT4, and CA-IX and loss of NIS expression [18, 32, 43, 44]. In vitro studies also suggested the influence of RAS mutations on [^{18}F]FDG uptake [45]. GLUT1 expression is also regulated by the PI3K/AKT/mTOR pathway, and in FTC, loss of function of PTEN increased the membrane expression of GLUT1 in vitro [46, 47]. Thus, at least a part of the benign nodules may carry genetic alterations that cause metabolic changes similar to those in thyroid carcinomas.

Hürthle cell neoplasms are considered a separate entity among the follicular cell-derived thyroid neoplasms. They are distinct in their clinical and biological behavior and carry different genetic alterations, primarily characterized by copy number alterations [48–50]. Malignant as well as benign Hürthle cell neoplasms are almost without exception strongly [^{18}F]FDG-positive, likely due to the abundance in mitochondria which is a typical feature of oncocytic cells [9, 51]. In two previous studies, the expression of GLUT1, HK2, MCT4, and CA-IX and the Ki-67 proliferation index were higher in Hürthle cell thyroid carcinoma and adenoma as compared to their non-oncocytic counterparts [19, 37]. In the current study, we included two Hürthle cell adenomas and two Hürthle cell carcinomas, all with high SUV_{max} (range 12.3 to 36.4 g/mL). Similar to literature, all four Hürthle cell lesions also showed remarkable and relatively strong expression of GLUTs, HK2, MCT4, and most other markers (Fig. 2).

In previous studies in thyroid cancer, correlations were established between various metabolic markers and signs of adverse prognosis. For example, GLUT1 overexpression was associated with tumor dedifferentiation, lymph node metastasis, and shorter overall survival [18, 22, 35, 36]. HIF1 α overexpression was associated with metastasis in FTC [17]. A high Ki-67 index was correlated with aggressive malignant behavior in both PTC and FTC [23, 37]. Loss of NIS expression was associated with tumor dedifferentiation [30, 43]. In Hürthle cell carcinoma, HK2 expression was associated with a tumor size larger than 4 cm, MCT4 with extrathyroidal tumor extension, and CA-IX with vascular invasion [19]. In the current study, only a limited number of thyroid carcinoma were included, and such prognostic correlations could not be assessed.

The main limitations of the current study were its case–control design, which is susceptible to selection bias, and its limited sample size. The latter limited the statistical power and may have caused underreporting of any effects. As the study was designed as a secondary and explorative analysis of data acquired during a randomized controlled trial, the current study was not powered in advance to

distinguish differences in immunohistochemical staining. In addition, during the interpretation of the data, it was assumed that the degree of immunohistochemical expression of metabolic markers positively correlated with the functional activity of these proteins. This assumption may not necessarily be correct and may be considered a general limitation of immunohistochemical studies. For example, immunohistochemical expression of NIS is not an accurate predictor of radioiodine uptake [29].

In conclusion, the positive correlations between [¹⁸F]FDG uptake and GLUT1, GLUT3, HK2, and MCT4 expression and differential expression of GLUT1, HK2, and MCT4 in [¹⁸F]FDG-positive benign thyroid nodules and [¹⁸F]FDG-positive thyroid carcinomas as compared to [¹⁸F]FDG-negative benign nodules in the current study suggest that these [¹⁸F]FDG-positive benign nodules undergo metabolic changes similar to those in thyroid carcinomas. Further studies in larger populations are required to confirm the findings of the current explorative study and unravel the underlying cellular mechanisms. A more extensive assessment, including a comparison of the genetic alterations, protein expression, and [¹⁸F]FDG-PET/CT results, could aid to connect genotype to phenotype. A separate analysis is recommended for Hürthle cell and non-Hürthle cell nodules.

Supplementary Information The online version contains supplementary material available at <https://doi.org/10.1007/s11307-022-01776-4>.

Acknowledgements The authors like to thank all the patients who participated in the *EffECTS* trial, all members of the *EffECTS* trial consortium, and all others who were involved in any of the study procedures, in particular Dr. Peter Laverman PhD, Head of the Radiopharmacy Unit and Research Labs, Department of Medical Imaging, Radboudumc, for his assistance with the immunohistochemical staining.

EffECTS Trial Study Group: Consortium Members

Romana T. Netea-Maier⁸, Jan W.A. Smit⁸, Johannes H.W. de Wilt⁹, Jan Booi¹⁰, Eric Fliers¹¹, Tamira K. Klooker¹¹, Eveline W.C.M. van Dam¹², Koen M.A. Dreijerink¹², Pieter G.H.M. Rajmakers¹³, Boen L.R. Kam¹⁴, Robin P. Peeters¹⁵, John F. Verzijlbergen¹⁴, Maarten O. van Aken¹⁶, Piet L. Jager¹⁷, G. Sophie Mijnhout¹⁸, Wilbert B. van den Hout¹⁹, Alberto M. Pereira Arias²⁰, Johannes Morreau²¹, Marieke Snel²⁰, Lioe-Ting Dijkhorst-Oei²², John M.H. de Klerk²³, Bas Havekes²⁴, D. Cristina Mitea²⁵, Stefan Vöö²⁵, Catharine B. Brouwer²⁶, Pieter S. van Dam²⁶, Ferida Sivro²⁷, Erik T. te Beek²⁸, Max C.W. Jebbink²⁹, Gysele S. Bleumink³⁰, Vanessa J.R. Schelfhout⁶, Ruth G.M. Keijsers³¹, Iris M.M.J. Wakelkamp³², Adrienne H. Brouwers³³, Thera P. Links³⁴, Bart de Keizer³⁵, Rachel S. van Leeuwen³⁶, Johannes J. Bonenkamp⁹, A. Rogier T. Donders³⁷, Jurgen J. Fütterer³⁸

⁸Department of Internal Medicine, Division of Endocrinology, Radboud University Medical Centre, Nijmegen, the Netherlands.

⁹Department of Surgical Oncology, Radboud University Medical Centre, Nijmegen, the Netherlands.

¹⁰Department of Radiology and Nuclear Medicine, Amsterdam University Medical Centers, Location Academic Medical Center, Amsterdam, the Netherlands.

¹¹Department of Endocrinology and Metabolism, Amsterdam University Medical Centers, Location Academic Medical Center, Amsterdam, the Netherlands.

¹²Department of Internal Medicine, Division of Endocrinology, Amsterdam University Medical Centers, Location VU Medical Center, Amsterdam, the Netherlands.

¹³Department of Radiology and Nuclear Medicine, Amsterdam University Medical Centers, Location VU Medical Center, Amsterdam, the Netherlands.

¹⁴Department of Nuclear Medicine, Erasmus University Medical Centre, Rotterdam, the Netherlands.

¹⁵Department of Internal Medicine, Erasmus University Medical Centre, Rotterdam, the Netherlands.

¹⁶Department of Internal Medicine, Haga Hospital, The Hague, the Netherlands.

¹⁷Department of Nuclear Medicine, Isala Hospital, Zwolle, the Netherlands.

¹⁸Department of Internal Medicine, Isala Hospital, Zwolle, the Netherlands.

¹⁹Department of Biomedical Data Sciences-Medical Decision Making, Leiden University Medical Center, Leiden, the Netherlands.

²⁰Department of Internal Medicine, Division of Endocrinology, Leiden University Medical Center, Leiden, the Netherlands.

²¹Department of Pathology, Leiden University Medical Center, Leiden, the Netherlands.

²²Department of Internal Medicine, Meander Medical Centre, Amersfoort, the Netherlands.

²³Department of Nuclear Medicine, Meander Medical Centre, Amersfoort, the Netherlands.

²⁴Department of Internal Medicine, Division of Endocrinology, Maastricht University Medical Centre, Maastricht, the Netherlands.

²⁵Department of Radiology and Nuclear Medicine, Maastricht University Medical Centre, Maastricht, the Netherlands.

²⁶Department of Internal Medicine, OLVG Hospital, Amsterdam, the Netherlands.

²⁷Department of Nuclear Medicine, OLVG Hospital, Amsterdam, the Netherlands.

²⁸Department of Nuclear Medicine, Reinier de Graaf Hospital, Delft, the Netherlands.

²⁹Department of Internal Medicine, Reinier de Graaf Hospital, Delft, the Netherlands.

³⁰Department of Internal Medicine, Rijnstate Hospital, Arnhem, the Netherlands.

³¹Department of Nuclear Medicine, St. Antonius Hospital, Nieuwegein, the Netherlands.

³²Department of Internal Medicine, St. Antonius Hospital, Nieuwegein, the Netherlands.

³³Department of Nuclear Medicine and Molecular Imaging, University Medical Centre Groningen, Groningen, the Netherlands.

³⁴Division of Endocrinology, Department of Internal Medicine, University Medical Centre Groningen, Groningen, the Netherlands.

³⁵Department of Radiology and Nuclear Medicine, University Medical Centre Utrecht, Utrecht, the Netherlands.

³⁶Department of Endocrine Oncology, University Medical Centre Utrecht, Utrecht, the Netherlands.

³⁷Department for Health Evidence, Radboud University Medical Centre, Nijmegen, the Netherlands.

³⁸Department of Medical Imaging, Radiology, Radboud University Medical Centre, Nijmegen, the Netherlands.

Author Contribution Lioe-Fee de Geus-Oei, Wim J.G. Oyen, and Dennis Vriens conceptualized the study. Lioe-Fee de Geus-Oei was the project leader. Wim J.G. Oyen and Dennis Vriens were principal investigators. Elizabeth J. de Koster was the junior investigator. All authors contributed to data acquisition and to the interpretation of the data. Elizabeth J. de Koster prepared the dataset for analysis, drafted the manuscript, and prepared the tables and figures. Elizabeth J. de Koster and Dennis Vriens verified the data and performed the statistical

analysis. All authors critically reviewed this manuscript, had full access to all the data in the study, and approved the manuscript before submission. Dennis Vriens had final responsibility for the decision to submit for publication.

Funding The *EFFECTS* trial, including the current study, was supported by a project grant from the Dutch Cancer Society (grant number KUN 2014–6514).

Declarations

Ethics Approval This study was performed in line with the principles of the Declaration of Helsinki. The *EFFECTS* trial, including the current study, was approved by the Medical Research Ethics Committee on Research Involving Human Subjects region Arnhem-Nijmegen, Nijmegen, the Netherlands on 10 November 2014.

Consent to Participate Prior to any study activities, written informed consent was obtained from all individual participants included in the study.

Consent for Publication All patients signed informed consent regarding publishing their data.

Conflict of Interest The authors declare no competing interests.

Open Access This article is licensed under a Creative Commons Attribution 4.0 International License, which permits use, sharing, adaptation, distribution and reproduction in any medium or format, as long as you give appropriate credit to the original author(s) and the source, provide a link to the Creative Commons licence, and indicate if changes were made. The images or other third party material in this article are included in the article's Creative Commons licence, unless indicated otherwise in a credit line to the material. If material is not included in the article's Creative Commons licence and your intended use is not permitted by statutory regulation or exceeds the permitted use, you will need to obtain permission directly from the copyright holder. To view a copy of this licence, visit <http://creativecommons.org/licenses/by/4.0/>.








References

- Boellaard R, Delgado-Bolton R, Oyen WJ et al (2015) FDG PET/CT: EANM procedure guidelines for tumour imaging: version 2.0. *Eur J Nucl Med Mol Imaging* 42:328–354
- Liberti MV, Locasale JW (2016) The Warburg effect: how does it benefit cancer cells? *Trends Biochem Sci* 41:211–218
- Piccardo A, Puntoni M, Dezzana M et al (2020) Indeterminate thyroid nodules. The role of (18)F-FDG PET/CT in the “era” of ultrasonography risk stratification systems and new thyroid cytology classifications. *Endocrine* 69:553–561
- Piccardo A, Puntoni M, Bertagna F et al (2014) 18F-FDG uptake as a prognostic variable in primary differentiated thyroid cancer incidentally detected by PET/CT: a multicentre study. *Eur J Nucl Med Mol Imaging* 41:1482–1491
- Santhanam P, Khthir R, Solnes LB, Ladenson PW (2018) The relationship of BRAF(V600e) mutation status to FDG PET/CT avidity in thyroid cancer: a review and meta-analysis. *Endocr Pract* 24:21–26
- Wang H, Dai H, Li Q, Shen G, Shi L, Tian R (2021) Investigating (18)F-FDG PET/CT parameters as prognostic markers for differentiated thyroid cancer: a systematic review. *Front Oncol* 11:1–9
- Choi JW, Yoon YH, Yoon YH, Kim SM, Koo BS (2011) Characteristics of primary papillary thyroid carcinoma with false-negative findings on initial (18)F-FDG PET/CT. *Ann Surg Oncol* 18:1306–1311
- Cibas ES, Ali SZ (2017) The 2017 Bethesda system for reporting thyroid cytopathology. *Thyroid* 27:1341–1346
- de Koster EJ, de Geus-Oei LF, Brouwers AH et al (2022) [18F] FDG-PET/CT to prevent futile surgery in indeterminate thyroid nodules: a blinded, randomised controlled multicentre trial. *Eur J Nucl Med Mol Imaging* 49:1970–1984
- van Berkel A, Rao JU, Kusters B et al (2014) Correlation between in vivo 18F-FDG PET and immunohistochemical markers of glucose uptake and metabolism in pheochromocytoma and paraganglioma. *J Nucl Med* 55:1253–1259
- Meyer HJ, Wienke A, Surov A (2019) Associations between GLUT expression and SUV values derived from FDG-PET in different tumors—a systematic review and meta analysis. *PLoS One* 14:e0217781
- de Geus-Oei LF, van Krieken JH, Aliredjo RP et al (2007) Biological correlates of FDG uptake in non-small cell lung cancer. *Lung Cancer* 55:79–87
- Kim MH, Ko SH, Bae JS et al (2013) Non-FDG-avid primary papillary thyroid carcinoma may not differ from FDG-avid papillary thyroid carcinoma. *Thyroid* 23:1452–1460
- Dierckx RA, Van de Wiele C (2008) FDG uptake, a surrogate of tumour hypoxia? *Eur J Nucl Med Mol Imaging* 35:1544–1549
- Busk M, Horsman MR, Jakobsen S, Bussink J, van der Kogel A, Overgaard J (2008) Cellular uptake of PET tracers of glucose metabolism and hypoxia and their linkage. *Eur J Nucl Med Mol Imaging* 35:2294–2303
- Schuurbiens OC, Meijer TW, Kaanders JH et al (2014) Glucose metabolism in NSCLC is histology-specific and diverges the prognostic potential of 18FDG-PET for adenocarcinoma and squamous cell carcinoma. *J Thorac Oncol* 9:1485–1493
- Klaus A, Fathi O, Tatjana TW, Bruno N, Oskar K (2018) Expression of hypoxia-associated protein HIF-1 α in follicular thyroid cancer is associated with distant metastasis. *Pathol Oncol Res* 24:289–296
- Nahm JH, Kim HM, Koo JS (2017) Glycolysis-related protein expression in thyroid cancer. *Tumour Biol* 39:1–10
- Kim HM, Koo JS (2017) Differential expression of glycolysis-related proteins in follicular neoplasms versus hurthle cell neoplasms: a retrospective analysis. *Dis Markers* 2017:6230294
- Meijer TW, Schuurbiens OC, Kaanders JH et al (2012) Differences in metabolism between adeno- and squamous cell non-small cell lung carcinomas: spatial distribution and prognostic value of GLUT1 and MCT4. *Lung Cancer* 76:316–323
- Kaida H, Kawahara A, Hayakawa M et al (2014) The difference in relationship between 18F-FDG uptake and clinicopathological factors on thyroid, esophageal, and lung cancers. *Nucl Med Commun* 35:36–43
- Grabellus F, Nagarajah J, Bockisch A, Schmid KW, Sheu SY (2012) Glucose transporter 1 expression, tumor proliferation, and iodine/glucose uptake in thyroid cancer with emphasis on poorly differentiated thyroid carcinoma. *Clin Nucl Med* 37:121–127
- Kjellman P, Wallin G, Hoog A, Auer G, Larsson C, Zedenius J (2003) MIB-1 index in thyroid tumors: a predictor of the clinical course in papillary thyroid carcinoma. *Thyroid* 13:371–380
- Itoh A, Iwase K, Jimbo S et al (2010) Expression of vascular endothelial growth factor and presence of angiovascular cells in tissues from different thyroid disorders. *World J Surg* 34:242–248
- Ryan HE, Poloni M, McNulty W et al (2000) Hypoxia-inducible factor-1 α is a positive factor in solid tumor growth. *Cancer Res* 60:4010–4015

26. Hoofst L, van der Veldt AA, van Diest PJ et al (2005) [18F]fluorodeoxyglucose uptake in recurrent thyroid cancer is related to hexokinase I expression in the primary tumor. *J Clin Endocrinol Metab* 90:328–334
27. Kaira K, Serizawa M, Koh Y et al (2014) Biological significance of 18F-FDG uptake on PET in patients with non-small-cell lung cancer. *Lung Cancer* 83:197–204
28. Qichang W, Lin B, Gege Z et al (2019) Diagnostic performance of 18F-FDG-PET/CT in DTC patients with thyroglobulin elevation and negative iodine scintigraphy: a meta-analysis. *Eur J Endocrinol* 181:93–102
29. Kollecker I, von Wasielewski R, Langner C et al (2012) Subcellular distribution of the sodium iodide symporter in benign and malignant thyroid tissues. *Thyroid* 22:529–535
30. Kim S, Chung JK, Min HS et al (2014) Expression patterns of glucose transporter-1 gene and thyroid specific genes in human papillary thyroid carcinoma. *Nucl Med Mol Imaging* 48:91–97
31. Kaida H, Hiromatsu Y, Kurata S et al (2011) Relationship between clinicopathological factors and fluorine-18-fluorodeoxyglucose uptake in patients with papillary thyroid cancer. *Nucl Med Commun* 32:690–698
32. Yoon M, Jung SJ, Kim TH et al (2016) Relationships between transporter expression and the status of BRAF V600E mutation and F-18 FDG uptake in papillary thyroid carcinomas. *Endocr Res* 41:64–69
33. Kim BH, Kim JJ, Kim SS, Kim SJ, Lee CH, Kim YK (2010) Relationship between biological marker expression and fluorine-18 fluorodeoxyglucose uptake in incidentally detected thyroid cancer. *Cancer Biother Radiopharm* 25:309–315
34. Lansoy-Kuhn C, Picquenot JM, Edet-Sanson A et al (2013) Relationship between the immunohistochemistry of the primary tumour and 18F-FDG-PET/CT at recurrence in patients with well-differentiated thyroid carcinoma. *Nucl Med Commun* 34:340–346
35. Ciampi R, Vivaldi A, Romei C et al (2008) Expression analysis of facilitative glucose transporters (GLUTs) in human thyroid carcinoma cell lines and primary tumors. *Mol Cell Endocrinol* 291:57–62
36. Yasuda M, Ogane N, Hayashi H et al (2005) Glucose transporter-1 expression in the thyroid gland: clinicopathological significance for papillary carcinoma. *Oncol Rep* 14:1499–1504
37. Mu N, Juhlin CC, Tani E et al (2018) High Ki-67 index in fine needle aspiration cytology of follicular thyroid tumors is associated with increased risk of carcinoma. *Endocrine* 61:293–302
38. Lloyd RV, Osamura RY, Klöppel G, Rosai J (2017) WHO classification of tumours of endocrine organs. WHO classification of tumours, 4th edn. IARC, Lyon, France
39. Remmele W, Stegner HE (1987) Recommendation for uniform definition of an immunoreactive score (IRS) for immunohistochemical estrogen receptor detection (ER-ICA) in breast cancer tissue. *Pathologe* 8:138–140
40. Demsar J, Curk T, Erjavec A et al (2013) Orange: data mining toolbox in Python. *J Mach Learn Res* 14:2349–2353
41. Matsuzo K, Segade F, Matsuzo U, Carter A, Bowden DW, Perrier ND (2004) Differential expression of glucose transporters in normal and pathologic thyroid tissue. *Thyroid* 14:806–812
42. Lewy-Trenda I, Wierchniewska-Lawska A (2002) Expression of vascular endothelial growth factor (VEGF) in human thyroid tumors. *Pol J Pathol* 53:129–132
43. Morari EC, Marcello MA, Guilhen AC et al (2011) Use of sodium iodide symporter expression in differentiated thyroid carcinomas. *Clin Endocrinol (Oxf)* 75:247–254
44. Zerilli M, Zito G, Martorana A et al (2010) BRAF(V600E) mutation influences hypoxia-inducible factor-1alpha expression levels in papillary thyroid cancer. *Mod Pathol* 23:1052–1060
45. Prante O, Maschauer S, Fremont V et al (2009) Regulation of uptake of 18F-FDG by a follicular human thyroid cancer cell line with mutation-activated K-ras. *J Nucl Med* 50:1364–1370
46. Morani F, Pagano L, Prodam F, Aimaretti G, Isidoro C (2012) Loss of expression of the oncosuppressor PTEN in thyroid incidentalomas associates with GLUT1 plasmamembrane expression. *Panminerva Med* 54:59–63
47. Heydarzadeh S, Moshtaghie AA, Daneshpoor M, Hedayati M (2020) Regulators of glucose uptake in thyroid cancer cell lines. *Cell Commun Signal* 18:83
48. Matsuura D, Yuan A, Wang LY et al (2022) Follicular and hurthle cell carcinoma: comparison of clinicopathological features and clinical outcomes. *Thyroid* 32:245–254
49. Corver WE, Demmers J, Oosting J et al (2018) ROS-induced near-homozygous genomes in thyroid cancer. *Endocr Relat Cancer* 25:83–97
50. Doerfler WR, Nikitski AV, Morariu EM et al (2021) Molecular alterations in Hurthle cell nodules and preoperative cancer risk. *Endocr Relat Cancer* 28:301–309
51. Pathak KA, Klönisch T, Nason RW, Leslie WD (2016) FDG-PET characteristics of Hurthle cell and follicular adenomas. *Ann Nucl Med* 30:506–509

Publisher's Note Springer Nature remains neutral with regard to jurisdictional claims in published maps and institutional affiliations.

Authors and Affiliations

Elizabeth J. de Koster¹  · Adriana C. H. van Engen-van Grunsven²  · Johan Bussink³  · Cathelijne Frielink¹ · Lioe-Fee de Geus-Oei^{1,4,5}  · Benno Kusters² · Hans Peters³  · Wim J. G. Oyen^{1,6,7}  · Dennis Vriens⁴  · On behalf of the EFFECTS trial study group

¹ Department of Medical Imaging, Nuclear Medicine, Radboud University Medical Centre, Nijmegen, the Netherlands

² Department of Pathology, Radboud University Medical Centre, Nijmegen, the Netherlands

³ Department of Radiation Oncology, Radiotherapy & OncoImmunology Laboratory, Radboud University Medical Center, Nijmegen, Netherlands

⁴ Department of Radiology, Section of Nuclear Medicine, Leiden University Medical Center, Leiden, the Netherlands

⁵ Biomedical Photonic Imaging Group, University of Twente, Enschede, the Netherlands

⁶ Department of Radiology and Nuclear Medicine, Rijnstate Hospital, Arnhem, the Netherlands

⁷ Department of Biomedical Sciences and Humanitas Clinical and Research Centre, Department of Nuclear Medicine, Humanitas University, Milan, Italy